Experimental Flow Field Investigation of the Bio-Inspired Corrugated Wing for MAV Applications

Y. D. DWIVEDI[1], ABHISHEK MOHAPATRA*,[1], T. BLESSINGTON[1], Md IRFAN[1]

*Corresponding author
[1]Department of Aeronautical Engineering, Institute of Aeronautical Engineering, Dundigal, Hyderabad, 500043, Telangana, India,
abhishekmohapatra@yahoo.com*

DOI: 10.13111/2066-8201.2021.13.2.5

Received: 17 August 2020/ Accepted: 28 April 2021/ Published: June 2021

Abstract: *This is an experimental flow field study of a bio-inspired corrugated finite wing from the dragonfly intended to assess the flow behavior over the wing and compare it with a wing of the same geometry with filled corrugation, at low Reynolds numbers 46000 and 67000. The work purpose is to explore the potential application of such types of wings for Micro Air Vehicles (MAVs) or micro sized Unmanned Air Vehicles (UAVs). Two types of wings are taken into account: first wing was a bio-inspired corrugated wing which was obtained from the mid span of the dragonfly, and the second wing was the same geometry with filled corrugation. Both wings were fabricated by using 3-D printing machine. The tufts were glued at three different locations i.e. at center, 30%, and 60% of the semi-span towards the right side of the wing at the trailing edge. The boundary layers were measured by using boundary layer rakes inside the open-end low speed wing tunnel with varied angles of attack. The results of the tuft flow visualization showed that the flow pattern at different span locations was different at different angles of attack and different wing velocities (Reynolds number). The fluctuations of the two different wings at the same angle of attack and Reynolds number were found different. Also, the directions of the flow for both wings were found to be different at different span locations. The boundary layer measurement results for both wings were found to be different at the same angles of attack and Reynolds numbers. The flow pattern also showed that the wing's upper as well as lower surface behaved differently on the same wing under the same measurement conditions. The results showed that the corrugated wing outperformed the conventional wing at low Reynolds number and the stall angle of the corrugated wing was more than the conventional wing.*

Key Words: *Finite wing, boundary layers, tuft flow visualization, stall angle, spanwise flow*

1. INTRODUCTION

For centuries, nature has inspired humans to fly like a bird or wander like an insect. However, till today humans have not been able to fly like the avian. The primary reason for this issue is the low Reynolds number (Re), on which the birds and insects normally operate. The extensive experimental and numerical studies have been conducted to understand the flow behavior and aerodynamic characteristics around the wings or airfoils at high Reynolds number, which corresponds to high speed and large size of the conventional available airplanes. On the other hand, in recent years, small sized air vehicles like Micro Air Vehicles (MAVs) and small sized Unmanned Air Vehicles (UAVs) have been developed to undertake tasks like aerial

photography, payload delivery, disaster management, monitoring hazardous places, etc. [1-3]. Car transportation is the main factor responsible for CO2 emissions that contribute to the greenhouse effect that causes serious environmental pollution [4, 5]. Nowadays, the UAVs, also known as drones, are extensively employed for delivery of goods and are able to save 90% of the energy while substantially reducing the greenhouse gases emission [6]. It is also observed that the flow field around the wings or airfoils of small aerial vehicles are significantly different from the conventional airplane wings and airfoils [7] because of low Reynolds number of the tiny flights ($Re<10^5$) [8, 9]. In high Re range, the inertial force prevails and trailing edge vortices are created, and flow becomes unstable, whereas at low Re, the viscous force is dominant and the flow remains stable as well as smooth. As a result, the performance of the stream lined low Reynolds number wings of MAVs/ UAVs/ birds/ insects etc., will degrade the performance significantly due to its small size and low velocity [10]. Hence, there is an imperative need to redesign the present conventional airfoils for the application of MAVs/UAVs to obtain better flow characteristics and aerodynamic performance in low Re regime. A dragonfly is an insect fit in to the family of *Odonata, anisoptera*, which is significantly fast, agile and has long endurance. This insect can be classified as low Reynolds number flier as the Re of the dragonfly falls between 10^2- 10^5 [11]. It can fly in gliding as well as flapping mode and also in combination of both [12]. In the flapping mode, the dragonfly is able to move forward, climb and also hover. However, the flapping requires significant energy consumption. So, the insect can't fly for long duration and switches to the gliding mode of the flight as this mode requires virtually little or no energy consumption at all [13]. This insect is unique in its efficient gliding flight as it is capable of flying 40 chord lengths and up to 30 seconds without any significant change in its altitude [14]. Unlike avian wings cross section, which is mostly smooth and cambered surface, the dragonfly wings cross section is found to be corrugated in chord as well as in spanwise direction. Several computational and experimental studies were performed to assess the aerodynamic behavior of corrugated wing and most of the investigations revealed that the corrugated wing performed at par and sometimes even better than the smooth conventional airfoils, especially at low Re flow regimes, in which the dragonfly mostly operates [15-24].

Many investigations have been made to understand the fundamental source of the unexpected improvement in the aerodynamic performance of the corrugated airfoils/ wings when compared with existing smooth wings. Kesel [12], Rees [13], and Murphy [19] observed that the corrugated airfoils/wings function as streamlined airfoil as the Leading Edge Vortices (LEVs) are trapped inside the trough of the valleys. This makes the flow to be streamlined, leading to the delay in separation [15, 21-22]. As a result, the lift is increased and drag is reduced thereby resulting in increased aerodynamic performance (L/D). Dwivedi et al [22, 23] has worked extensively on the experimental study of the flow field around the corrugated airfoils at low Re and observed that the spanwise flow and boundary layers were significantly different from the conventional smooth wings. Luo and Sun [16] have investigated the effect of corrugation on generation of the aerodynamic forces and Vergas and Mittal [18] have done the computational study to assess the aerodynamic performance and have found that the corrugation gives better performance than the smooth profile wing. Tang et al [20] have worked computationally for 3-D wing and concluded that spanwise flow direction could promote the lift and decrease the drag. They have also confirmed that the wings are unstable and the same results have been obtained by Dwivedi et al. [21]. Despite different explanations about the flow field mechanism for the improved aerodynamic performance by the different investigators, all studies unanimously agree that the corrugation of the wing works well in low Re regime, which indicates that the bio inspired corrugated wings can be potentially used for

the wings of future MAVs/UAVs applications.

It should be noted that there are several numerical as well as experimental investigations on assessing the aerodynamic performance of the corrugated dragonfly airfoils/wings, but there are very few studies about the flow field visualization to assess the drag, flow separation and flow reversal. These parameters are essential to estimate the aerodynamic behavior and to understand the underlying mechanism and physics behind the more lift and less drag produced by the bio inspired corrugated wings. The flow separation and flow reversal have been experimentally observed by Tamai et al [25]. The computational result of Skote [26, 27] and Chen and Skote [28] have revealed that the spanwise flow does exist in the corrugated wings and 3-D flow field persists. Flow separation occurs, when the thickness of the boundary layer exceeds the critical value which results in the adverse pressure gradient (APG) and the growth of the boundary layers relative to the object surface falls almost zero. The fluid flow detaches from the surface of the object and forms eddies and vortices. Flow separation occurs when flow actually reverses. Most of the earlier investigations only focused on comparing the camber as well as the thickness of corrugated wings with that of either the flat plate or NACA airfoils or both. However, those comparisons are unrealistic. First, the flat plate does not even have the camber; second, NACA airfoil geometry is starkly different from that of bio-inspired corrugated wings. So, the previous results obtained, either computationally or experimentally, may not be matching with real bio inspired corrugated wings.

The present paper aims to experimentally investigate the flow behavior of a bio inspired corrugated wing and to compare the results with another wing having same thickness, camber, chord, and aspect ratio with varying AOA and two Reynolds numbers 46000 and 67000. The flow phenomena of both tested wings were visualized by using tufts and boundary layers were measured by using boundary layer rake at three different semi-span locations in a low speed wind tunnel at 0.7 chord length (70%) from the leading edge of the wing. The flow visualization and boundary layer study gave the clear understanding of the underlying flow mechanism of the bio inspired corrugated wing and the wing can be assessed for the suitability to the MAVs/UAVs application.

2. METHODOLOGY

2.1 Materials and methods

Two different wing models are used in the present study: (1) Corrugated wing and (2) Hybrid wing. Both wing models have the same projected planform area (S), mean chord length (c) and aspect ratio (AR). The construction and design of the profile are based on the real time analysis of the wing structure of the biological dragonfly under microscopic observation and plotting the spatial locations of the elements of the geometry with respect to the mean chord line of the wing. All the co-ordinates of the points for corrugated and hybrid profile are given in table 1 and 2, respectively for plotting, design, analysis, and fabrication purposes.

Table 1. Coordinates of corrugated wing profile

UPPER SURFACE		LOWER SURFACE	
x/c	y/c	x/c	y/c
0	0.02	0.995	-0.02
0.066	0.02	0.912	-0.005
0.124	0.058	0.833	0
0.189	0.016	0.77	-0.028
0.271	0.073	0.688	0.001

0.341	0.013	0.606	-0.027
0.398	0.051	0.537	0.014
0.553	0.051	0.415	0.014
0.61	0.015	0.337	-0.03
0.689	0.043	0.272	0.023
0.772	0.014	0.187	-0.029
0.839	0.032	0.128	0.01
0.897	0.036	0.08	-0.02
1.005	0.02	0	-0.02

Table 2. Coordinates of hybrid wing profile

UPPER SURFACE		LOWER SURFACE	
x/c	y/c	x/c	y/c
0	0.02	0.995	-0.02
0.066	0.02	0.912	-0.005
0.124	0.058	0.833	0
0.271	0.073	0.688	0.001
0.398	0.051	0.537	0.014
0.553	0.051	0.415	0.014
0.689	0.043	0.337	-0.03
0.839	0.032	0.187	-0.029
0.897	0.036	0	-0.02
1.005	0.02		

The co-ordinates (table 1 and 2) utilized for plotting the wing geometry (Fig.1) are gathered from various pre-existing sources and are spatially multiplied by the suitable integral constants (1:100 scale-up) for a noticeable geometry to carryout aerodynamic analysis using the Wind tunnel and obtain significant results.

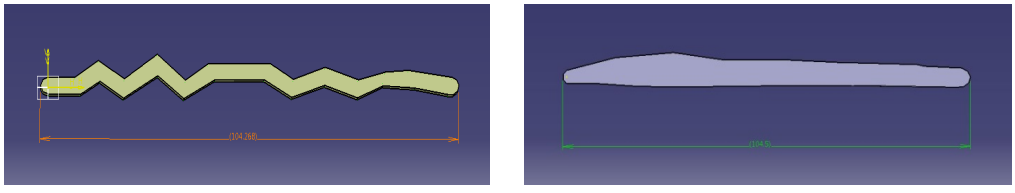

Figure 1: Geometry of Corrugated Wing and Hybrid Wing

2.1.1 Numerical adjustments and curve fittings

The profile co-ordinates were refined for plotting a suitable corrugated and hybrid wing models for analysis purpose. The real time wings of dragonfly are too small and to model accurately to its original dimensions would not yield satisfactory results for the wind tunnel testing. The Wing Tunnel test section (60cmx60cmx200cm) is quite massive in magnitude compared to that of a real corrugated wing model of a Dragonfly.

Such a relatively small wing model would not induce any noticeable disturbances or any significant changes in the free stream flow in the test section. Hence, geometrical enhancements were made to the miniature real dimensions to scale-up (1:100) the reference model to produce significant variations and flow disturbances in the free stream flow within the test section.

Thus, the measurement of the deviations in the flow patterns can be clearly observed and can be further carefully analyzed.

a) Corrugated Wing b) Hybrid Wing

Figure 2: CATIA 3D Model of Corrugated and Hybrid wings

The geometrical aberrations are of magnitudes less than 0.15% error to the total dimensions of the model. These profiles were plotted using the aid of the design and modeling software CATIA V5. The generated model was then converted into (.stl) format (stereo lithography) and G-Code format (RS-274) under standard ISO 6983 conditions. This data of refined co-ordinates was then used to produce a 3D printed model of ABS (Acrylonitrile Butadiene Styrene) thermoplastic material as shown in figure 4. Model specification includes Chord length (c) 105.4 mm, Wing span 205.4 mm, Effective thickness 4 mm, and Camber 0.17 c. The 3D printing machine (Ultimaker Cura^{TM} 3+) was used to fabricate the model as shown in figure 3.

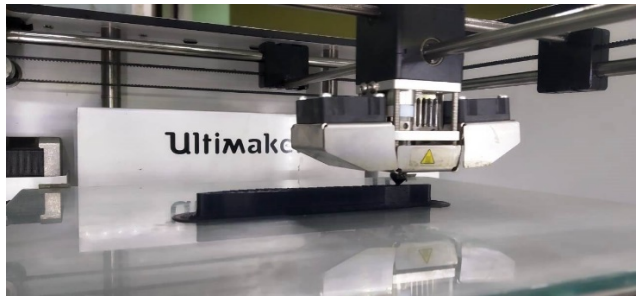

Figure 3: 3D Printing of wings using Ultimaker Cura 3+

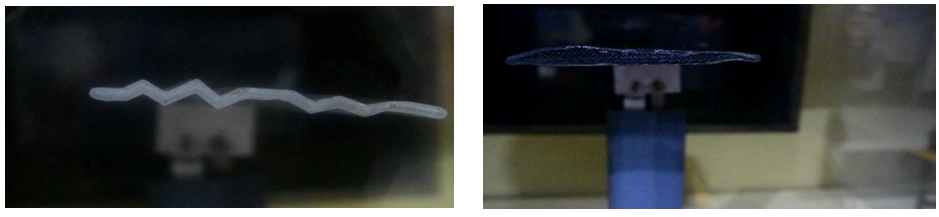

Figure 4: 3D Printed wings mounted on six component balance

2.2 Experimental setup

The low speed subsonic wind tunnel facility from Department of Aeronautical Engineering, Institute of Aeronautical Engineering, Hyderabad, India was used for experiment (Fig.7). It has a test section of 0.6 m x 0.6 m x 2 m dimension and produces a maximum free stream velocity of 50 ms^{-1}. This speed is obtained by an axial flow fan of diameter 1.3 m with 12 number of fan blades at 1475 RPM. The ratio of contraction is 9:1, length of contraction 1.8 m, dimension of settling chamber is 1.8 m x 1.8 m, dimension of honey comb is 0.025 m x 0.025 m x 0.200 m. The inclined tube manometer (fig. 5) is used for velocity and pressure measurement. Both the limbs of the manometer are attached to the static pressure holes, one in the settling chamber just before contraction part and the other to that at the beginning of the test section. The manometer reading is the dynamic head of fluid in the test section and it functions as reference for maintaining the tunnel speed constant. Inclination of the manometer

is set 30^0 to the horizontal; at this angle the change in the liquid (methanol) column length is twice to the vertical head, which gives better accuracy. Wind tunnel is also equipped with Pitot-static tube, which can be navigated across the tunnel section. The fan is connected with adjustable speed motor, which is varied by three phase AC controller and motor with suitable power source. The wind tunnel is well equipped with pressure distribution measuring system, multi tube manometer (Fig. 5), six-component force balance system and seventeen probe boundary layer measuring rake (Fig. 6). Both 3D printed wing models were fixed in the test section (Fig. 4) along with the boundary layer measuring probes and manometer to record the readings. The wind tunnel can run at extreme free stream velocity of 50 m/s, the AOA can be varied from -20^0 to $+20^0$ with an accuracy of $\pm 0.5^0$, in this work the exact AOA were set using digital inclinometer with accuracy ± 0.10. However, a similar kind of experimental setup was used by Dwivedi et al. [24].

Figure 5: Inclined tube manometer

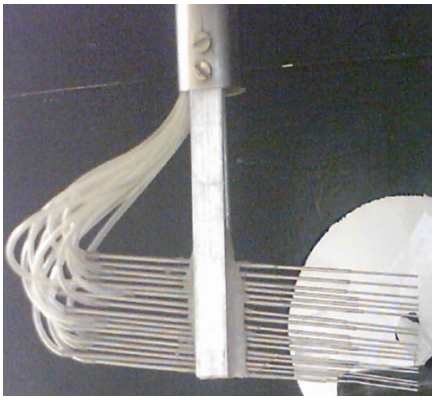

Figure 6: Boundary Layer Measuring Rake

Figure 7: Full Experimental Setup

3. RESULTS AND DISCUSSIONS

3.1 Tuft Flow visualization

Three different coloured tufts were used for both wings tuft flow visualization. Black tuft is fixed at center of the wing (0%) of semi-span (BT 0), Red tuft at 30% of semi-span (RT 30) and a Green tuft at 60% of semi-span (GT 60), which is near the tip of the wing. The experiment was carried out at two chord Reynolds number (Re_c) 46000 and 67000 and angle of attack (AOA) varied from -20 degree to +20 degrees for both the wings. Chord Reynolds number (Re_c) calculations are given in table 3. The green tuft (GT 60) located at 60% of semi-span towards the tip showed more fluctuations than that of the other two, while remaining two

i.e. BT 0 and RT 30 reacted almost similar to the flow (Fig 8 and 9).This showed that the flow fluctuation at low Re_c (46000 and 67000) and Low AOA (<6 degree) is high towards the tip of the wing. The flow behavior of the corrugated wing found to have changed as the AOA is increased gradually to +6 degrees and Re_c to 120,000. The Red tuft is observed to flutter at very high amplitude but no sign of flow reversal is observed at the same AOA. At the AOA +7 degree and Re_c 120,000 a momentary reversal of Red tuft is observed, which didn't last long. At the same Re_c and AOA +14 degree, a permanent flow reversal of Black tuft is happened followed by Red and Green tufts in corrugated wing (Fig.10) while increasing the AOA slowly. In Hybrid wing the same phenomena showed at +18 degree AOA and Re_c 120000 (Fig.11). Although heavy flutter of the Red tuft is commonly observed at -7 and -9 degree AOA and Re_c 120,000 on corrugated wing the complete flow reversal of Green tuft occurred followed by Red and black at -10 degree AOA. The same occurred in Hybrid wing at -14 degree AOA (Fig.12 and 13). This showed that the flow reversal of the hybrid wing is delayed by 4 degrees which is a significant advantage over the corrugated wing. At high AOA in negative and positive after flow reversal and separation the vortices were observed in which the flow was moving towards the center of the wing.

Table 3. Chord Reynolds Number (Re_c) calculation

Wind Tunnel motor RPM	Chord [m]	Wind Tunnel velocity [m/s]	Kinematic viscosity [m^2/s]	Chord Reynolds No. [Re_c] (approx.)
265	0.104	6.9089	1.562×10^{-5}	46,000
370	0.104	10.0629	1.562×10^{-5}	67,000

For corrugated wing with a high AOA and Rec around 120,000 the flow reversal was observed. This was however already shown by Chen and Skote [27], & Dwivedi et al. [23] but their Re_c was different. As the AOA was associated with the Re_c in this phenomenon, their corresponding AOA was also different.

Figure 8: Tuft flow visualization for Corrugated wing at AOA+4 degree and Re_c 67000

Figure 9: Tuft flow visualization for Hybrid wing at AOA+4 degree and Re_c 67000

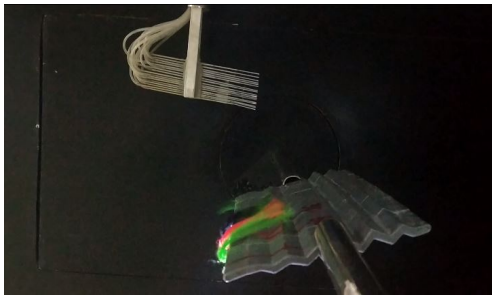

Figure 10: Flow reversal for Corrugated wing at AOA $+14^0$ and Re_c 120000

Figure 11: Flow reversal for Hybrid wing at AOA $+18^0$ and Re_c 120000

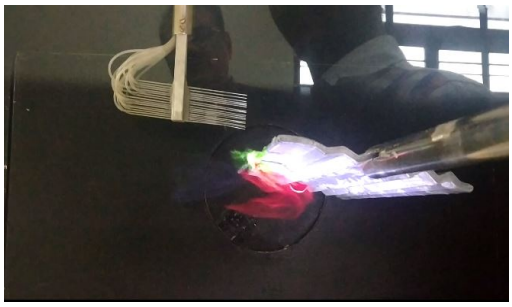

Figure 12: Flow reversal for Corrugated wing at AOA -10^0 and Re_c 120000

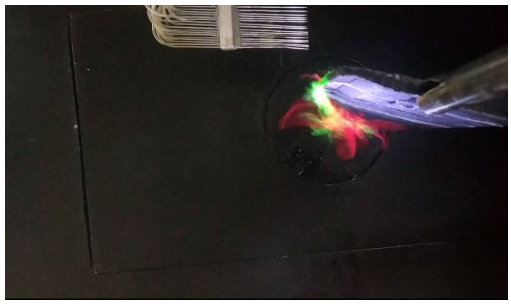

Figure 13: Flow reversal for Hybrid wing at -14^0 AOA and Re_c 120000

3.2 Boundary layer measurements

In above discussion the qualitative tuft flow visualization was undertaken to find the reversal and separation of flow for both wings. However, to find the exact reason which causes separation, reversal and swirling of the flow (a directional rotation of flow), a measurement technique was needed. That technique is the boundary layer measurement. In measuring the boundary layer the target was to obtain the velocity profile above the two tested wing surfaces at 70% chord length (0.7 c) from the leading edge and at three different locations at 0%, 30%, and 60% from the center of the wing. A 17 probe boundary-layer measuring rake (Fig. 6) is used to measure the velocity profile. The location of the probes is provided in table 4. The probes were connected to a manometer filled with methanol and aligned perpendicular to the ground, the perpendicular alignment is verified by two-spirit balances attached to the base of the manometer, perpendicular to each other and parallel to the ground. The velocity field around the wing surface creates the pressure difference between the upper and the lower surfaces. However, the variation in the velocity field is not the same for both the corrugated and the hybrid wing. A negative pressure is generated on the upper surface of the corrugated wing. The corrugation present at the lower surface acts like a wing camber. In the case of the hybrid wing although the behavior of the flow was not alike the corrugated one there was not much difference too. The flow behavior observed is completely governed by parameters like chord length, the thickness of profile, AOA, and the relative velocity across the surface of the profile which is responsible for turbulent flow, flow separation, and flow reversal.

In this measurement setup, only 17 probes of the boundary-layer measuring rake were used. These probes were connected with transparent flexible pipes and steel unions. In this setup, the bottom-most probe was the first probe, which was just touching the wing surface, representing the no-slip condition.

The distance between the first and the last probe was 35mm and spaced as per the standards. The boundary layer was measured in Re_c and AOA ranging from -8^0 to + 16^0. The result obtained for both wings is thoroughly reviewed and verified.

Table 4. Boundary Layer Rake Device Probe Numbers and Distances

Tube No.	Distance	Tube No.	Distance
1	0 mm	10	14.5 mm
2	1.5 mm	11	16.5 mm
3	2.5 mm	12	20.0 mm
4	4.5 mm	13	22.5 mm
5	5.5 mm	14	24.5 mm
6	7.0 mm	15	27.0 mm
7	8.5 mm	16	31.0 mm

8	10.5 mm	17	34.5 mm
9	12.0 mm		

At AOA -8^0 and Re_c 46000 or 67000 there is no significant difference in velocity profile of corrugated wing at 0%, 30%, and 60% of the wing semi-span . In the same condition, also no significant difference in velocity profile is observed between 0%, 30%, and 60% of the hybrid wing semi-span too, but the average boundary layer (BL) thickness at 67000 is greater than that of at 46000 (Fig. 14-15). Further, the hybrid wing velocity profile at 0% of semi wingspan remained higher in comparison with corrugated wing till probe number 9 (thicker boundary layer).

At AOA 0^0 and Re_c 46000 a very thin boundary layer is observed for corrugated wing which lasted up to only 3 probes for all the 3 locations. When the Re_c increased to 67000 a comparatively thicker boundary layer is observed. It lasted up to 5 probes. The highest velocity is recorded at 30% of semi wing span. At the same AOA and Re_c 46000 the hybrid wing experienced a thick boundary layer which lasted up to approximately 7^{th} probe. When the Re_c increased to 67000 the BL thickness increased up to 8^{th} probe. The flow behaved similarly at each 3 locations discussed previously (Fig.16-17).

At 4^0 AOA and chord Reynolds number at 46,000 the corrugated wing velocity profile at 30% of the semi wing span observed to be less than and that of the other two positions. Keeping all the other parameters same and varying the Re_c to 67,000, it has been observed that the velocity profile at 0% of the semi wingspan is the highest among all (up to probe number 9) which represents a comparative thick boundary layer followed by the velocity profile at 30% and 60% respectively. The hybrid wing at the 4^0 AOA and Re_c 46,000 the boundary layer thickness is highest at 60% of the semi-span i.e. up to probe number 8, followed by 30% and 0% of the semi-span, respectively.

However, increasing the Re_c up to 67,000 resulted in the thickest boundary layer at 60% of the wing semi-span up to 14^{th} probe, followed by 30% of the semi-span and 0% of the semi-span, respectively (Fig. 18-19).

At 16^0 AOA and at Re_c 46,000 where the wing was in a complete stall condition, it was observed for the corrugated wing that there is a difference in velocity profile between 0% of the semi-span and 60% of the semi-span. The pressure drop at 0% of the semi-span was more than that of 60% of the semi-span. When the Re_c of the wind tunnel increased gradually and reached at 67,000 the velocity profile difference increased drastically between the same and a rotation of flow is observed (Fig. 20-21).

A thick boundary layer was witnessed at both the Re_c (up to probe number 12) for 0% of the semi-span followed by 30% and the least for 60% of the semi-span. For the hybrid wing at above conditions and Re_c at 46,000 no much difference in velocity profile is observed between 0%, 30% it and 60% of the semi-span but unlike the corrugated wing A thicker boundary layer is witnessed at 60% of the semi-span followed by 30% and 0% of semi-span . Overall, it has been constantly observed that the hybrid wing always exhibited the property of thick boundary layer at all tested Re_cs at 46,000 & 67,000, and AOA ranging from -8 degree to +16 degrees than that of the corrugated wing.

The contrasting character between the two wings in some cases is observed that for corrugated wing the boundary layer at the center of the wing is thicker than that of at 60% of the wing semi-span whereas for the hybrid wing the boundary layer is thicker at 60% than that of at the center of the wing.

Also, unlike the corrugated wing, the hybrid wing has never witnessed a high span wise difference in the velocity profile. Thus, the flow rotation or swirling is always weaker in the case of the hybrid wing when compared with the corrugated wing.

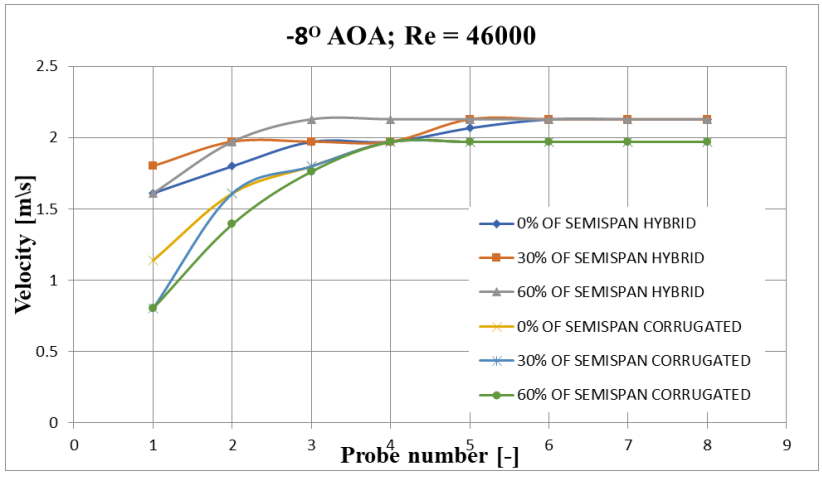

Figure 14: Comparison of Boundary Layer Velocity at -8^0 AOA and Re_c=46000

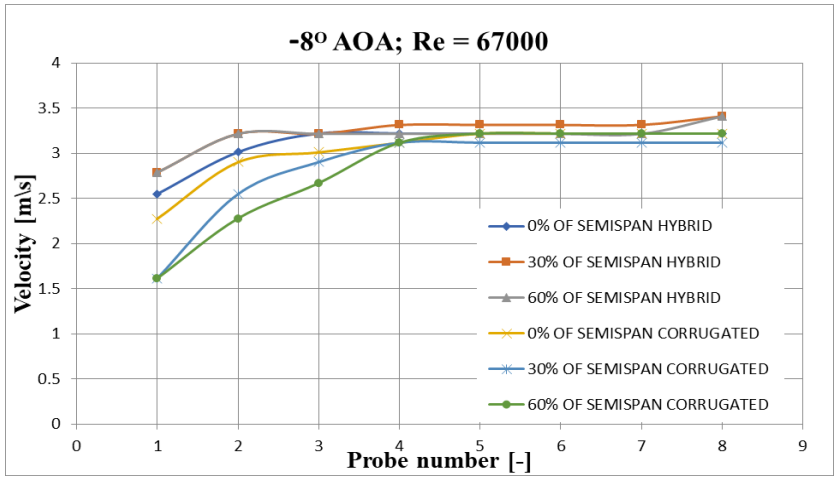

Figure 15: Comparison of Boundary Layer Velocity at -8^0 AOA and Re_c=67000

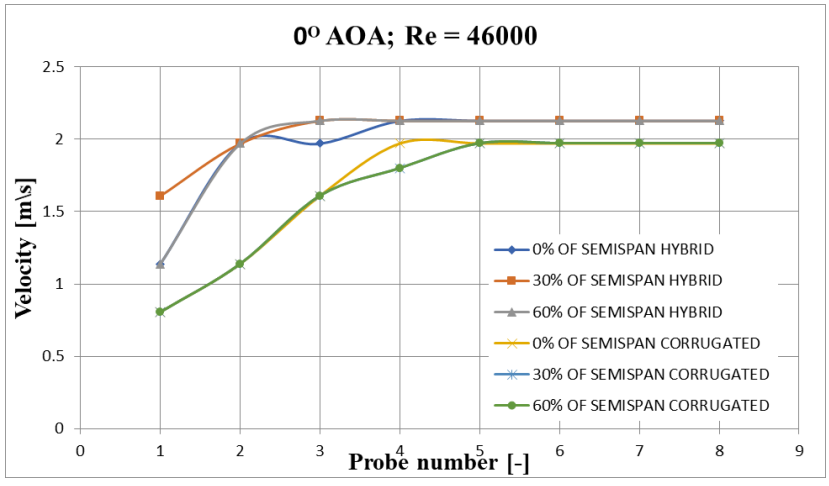

Figure 16: Comparison of Boundary Layer Velocity at 0^0 AOA and Re_c=46000

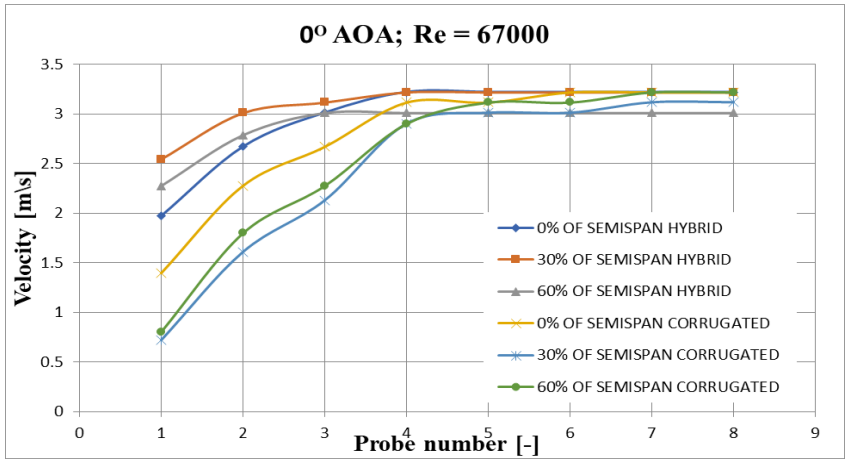

Figure 17: Comparison of Boundary Layer Velocity at 0^0 AOA and Re_c=67000

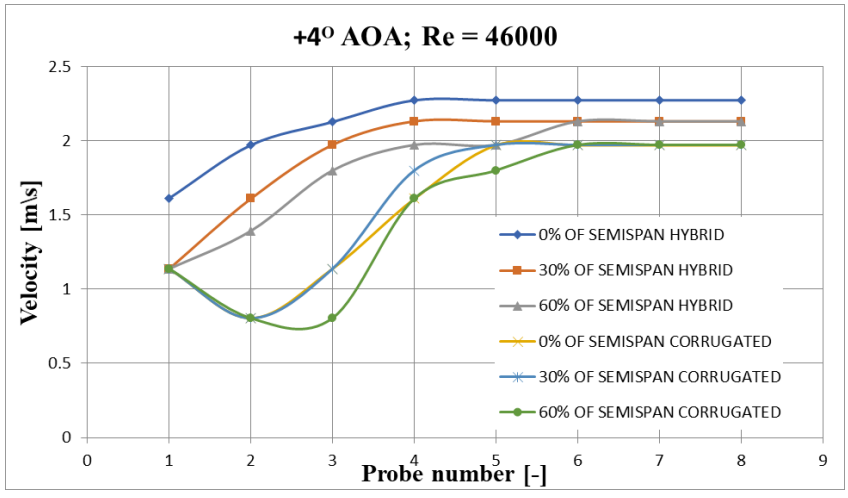

Figure 18: Comparison of Boundary Layer Velocity at $+4^0$ AOA and Re_c=46000

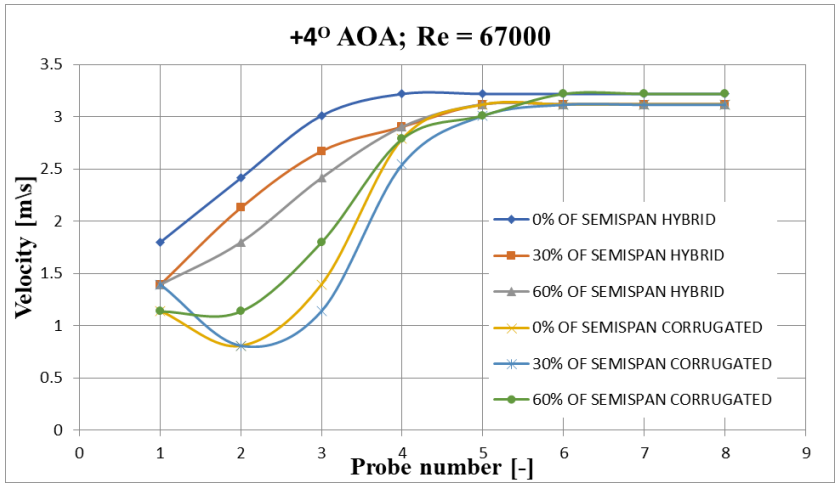

Figure 19: Comparison of Boundary Layer Velocity at $+4^0$ AOA and Re_c=67000

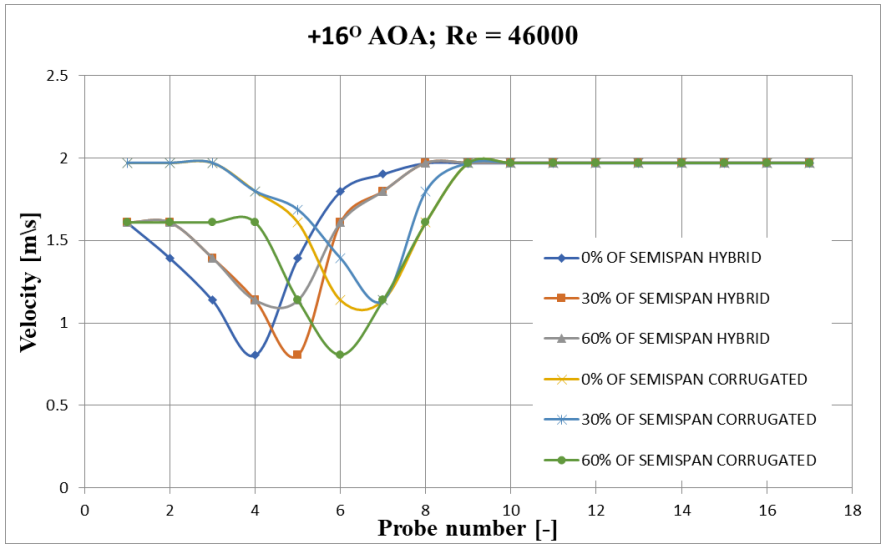

Figure 20: Comparison of Boundary Layer Velocity at $+16^0$ AOA and Re_c=46000

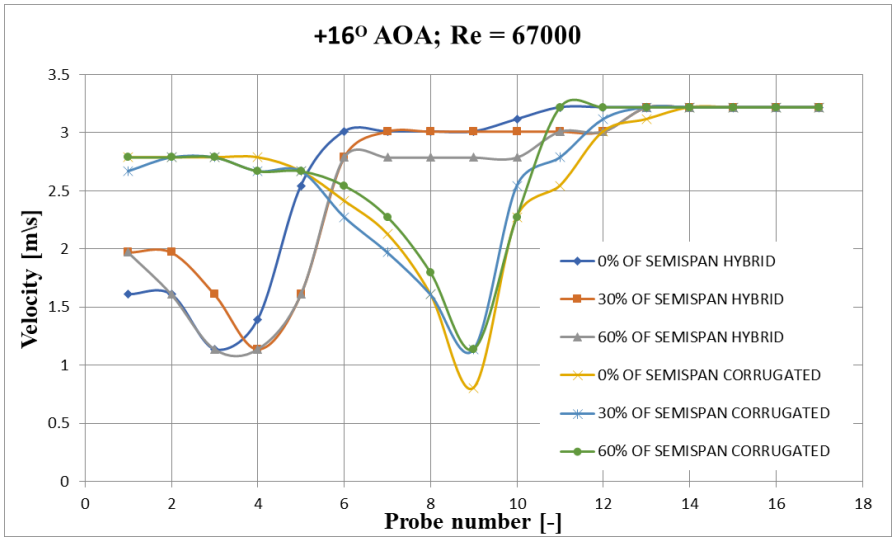

Figure 21: Comparison of Boundary Layer Velocity at $+16^0$ AOA and Re_c=67000

4. CONCLUSIONS

No flow reversal and flow separation are observed for the two wings at the Re_c 46,000 or 67,000 and angles of attack from -8 degrees to +16 degrees. But when the Chord Reynolds number (Re_c) was increased extremely, at around 120,000 (Fig. 10-13) the corrugated wing encountered a flow reversal for a black tuft at +14 degrees followed by red and green tuft. At negative AOA the green tuft of the corrugated wing witnessed the first complete flow reversal at -10 degree followed by the red and black tuft. This paper offers the same results as those in the study of Tamai et al., 2007 [25] where the flow separation and flow reversal were experimentally observed.

At the same Re_c, the hybrid wing experienced the flow reversal first for the black tuft at +18 degrees AOA followed by red and green tuft. At the negative AOA first, the green tuft

witnessed a flow reversal at -14 degree AOA followed by the red and black tuft. However, at around +21 degree and -18 degree AOA, both wings experienced a complete flow reversal. The thickest boundary layer up to probe 14th for the hybrid wing is observed at an AOA +4 degrees and Re_c 67000 at 60% of the wing semi-span. And for the corrugated wing, it is up to 12th probe experienced at the AOA +16 degrees and Re_c 67000 at 60% of the wing semi-span.

REFERENCES

[1] A. Mohiuddin, T. Taha, Y. Zweiri, D. Gan, UAV payload transportation via RTDP based optimized velocity profiles, *Energies*, **12** (16), 30-49, 2019, https://doi.org/10.3390/en12163049.

[2] J. Estevez, J. M. Lopez-Guede, M. Grana, Quasi-stationary state transportation of a hose with quadrotors, *Robot. Auton. Syst.*, **63**,187–194, 2015, https://doi.org/10.1016/j.robot.2014.09.004.

[3] * * * *Wall Street Journal*, Google Drones Can Already Deliver You Coffee in Australia, Available online: https: //www.youtube.com/watch?v=prhDrfUgpB0 (accessed on 6 April 2019).

[4] J. Koiwanit, A. Manuilova, C. Chan, et al., A life cycle assessment study of a hypothetical Canadian oxy-fuel combustion carbon dioxide capture process, *International J. GHG Con.*, **28, 25**7-274, 2014, https://doi.org/10.1016/j.ijggc.2014.07.001

[5] J. K. Stolaroff, C. Samaras, E. R. O'Neill, A. Lubers, A. S. Mitchell, D. Ceperley, Energy use and life cycle greenhouse gas emissions of drones for commercial package delivery, *Nat. Commun.*, **9**, 409, 2018.

[6] J. Liu, Z. Guan, J. Shang, X. Xie, Analysis of environmental impacts of drone delivery on an online shopping system, *Journal of Systems Science and Information Aug.*, Vol. **6**, No. 4, pp. 302–319, 2 DOI: 10.21078/JSSI-2018-302-18, 2018.

[7] J. H. McMasters and M. L. Henderson, Low Speed Single Element Airfoil Synthesis, *Tech. Soaring*, Vol. **2**, No. 2, 1980: 1-21.

[8] B. H. Carmichael, Low Reynolds Number Airfoil Survey, Volume **1**; NASA CR-165803; NASA: Washington, DC, USA, 1981.

[9] P. B. H. Lissaman, Low-Reynolds-number airfoils, *Annu. Rev. Fluid Mech.*, **15**, 223–239, 1983.

[10] M. Gad-el-Hak, Micro-air-vehicles: Can they be controlled better? *J. Aircr.*, **38**, 419–429, 2001.

[11] J. M. Wakeling, C. P. Ellington, Dragonfly flight I. Gliding flight and steady-state aerodynamic forces, *J. Exp. Biol.*, **200**, 543–556, 1997.

[12] A. B. Kesel, Aerodynamic characteristics of dragonfly wing sections compared with technical aerofoil, *J. Exp. Biol.*, **203**: 3125–3135, doi.org/10.1016/S0010-4825 (98)018-3, 2000.

[13] C. J. C. Rees, Aerodynamic properties of an insect wing section and a smooth aerofoil compared, *Nature*, **258**: 141–142, 1975.

[14] A. K. Brodsky, *The Evolution of Insect Flight*, Oxford University Press: Oxford, UK, 1994.

[15] R. Rudolph, Aerodynamic properties of Libellula quadrimaculata L. (Anisoptera: Libellulidae), and the flow around smooth and corrugated wing section models during gliding flight, *Odonatologica*, **7**, 49–58, 1978.

[16] M. Okamoto, K. Yasuda and A. Azuma, Aerodynamic characteristics of the wings and body of a dragonfly, *J. Exp. Biology*, **199**: 281-294, 1996.

[17] G. Luo, and M. Sun, The effects of corrugation and wing planform on the aerodynamic force production of sweeping model insect wings, *Acta Mech. Sin.*, **21**, 531–541, 2005.

[18] A. Vargas and R. Mittal, Aerodynamic Performance of Biological Airfoils, *Proceedings of 2nd Flow Control Conference*, Portland, Oregon, AIAA2004-2319, doi.org/10.2514/6.2004-2319, 2004.

[19] J. Murphy and H. Hu, An experimental study of a bio inspired corrugated airfoil for micro air vehicle applications, *Exp Fluids*, **492**: 531–546, doi:10.1007/s00348-010-0826-z., 2010.

[20] H. Tang, Y. Lei, X. Li and Y. Fu, Numerical Investigation of the Aerodynamic Characteristics and Attitude Stability of a Bio-Inspired Corrugated Airfoil for MAV or UAV Applications, *Energies*, **12**: 4021, doi: 10.3390/en12204021, 2019.

[21] Y. D. Dwivedi, Vasishta Bhargava, P. M. V. Rao and Donepudi Jagadeesh, Aerodynamic Performance of Micro Aerial Wing Structures at low Reynolds Number, *INCAS BULLETIN*, **11**(1): 107-120, doi: 10.13111/2066-8201.2019.11.1.8, 2019.

[22] Y. D. Dwivedi and Y. B. Sudhir Sastry, An experimental Flow Field Study of a Bio-inspired Corrugated Wing at Low Reynolds number, *INCAS BULLETIN*, **11**(3): 55-65, doi: 10.13111/2066-8201.2019.11.3.5, 2019.

[23] Y. D. Dwivedi, W. H. Ho, and P. M. V Rao, Spanwise Flow Analysis of Gliding Bio-inspired Corrugated Wing, *Jour of Adv. Research in Dynamical & Control Systems*, **12** - Special issue, August 2017.

[24] Y. D. Dwivedi, Effect of Peak Shape in Bio Inspired Corrugated Wing, International Conference on Advances in Thermal Systems, *Materials and Design Engineering* (ATSMDE2017), VJTI, Mumbai, India, 21 Dec 2017.
[25] M. Tamai, Z. Wang, G. Rajagopalan, H. Hu, and G. He, Aerodynamic performance of a corrugated dragonfly airfoil compared with smooth airfoils at low Reynolds numbers, *45th AIAA Aerospace Sciences Meeting and Exhibit*, 1-12, 2007.
[26] M. Skote, Scaling of the velocity profile in strongly drag reduced turbulent flows over an oscillating wall, *I. J of Heat and Fluid Flow*, **50**: 352–358, 2014.
[27] M. Skote, Turbulent boundary layer flow subjected to stream wise oscillation of spanwise wall-velocity. *Physics of Fluids,* **23**, 1701-1704, 2011.
[28] Y. H. Chen and M. Skote, Gliding performance of 3-D corrugated dragonfly wing with spanwise variation, *Journal of Fluids and Structures,* **62**: 1-13, 2016.